Two-dimensional $S=\frac{1}{2}$ Heisenberg antiferromagnets: Synthesis, structure, and magnetic properties

F. M. Woodward, A. S. Albrecht, C. M. Wynn, and C. P. Landee
Department of Physics, Clark University, Worcester, Massachusetts 01610

M. M. Turnbull
Carlson School of Chemistry and Biochemistry, Clark University, Worcester, Massachusetts 01610

(Received 22 August 2001; published 27 March 2002)

The magnetic susceptibility and magnetization of two layered $S=\frac{1}{2}$ Heisenberg antiferromagnets with moderate exchange are reported. The two isostructural compounds, (2-amino-5-chloropyridinium)$_2$CuBr$_4$ [(5CAP)$_2$CuBr$_4$] and (2-amino-5-methylpyridinium)$_2$CuBr$_4$ [(5MAP)$_2$CuBr$_4$], contain $S=\frac{1}{2}$, Cu(II) ions related by C centering, yielding four equivalent nearest neighbors. The crystal structure of the synthesized compound, (5CAP)$_2$CuBr$_4$, shows the existence of layers of distorted copper(II)-bromide tetrahedra parallel to the ab plane, separated by the organic cations along the c axis. Magnetic pathways are available through the bromide-bromide contacts within the layers and provide for moderate antiferromagnetic exchange. Susceptibility measurements indicate interaction strengths to be 8.5(2) K and 6.5(2) K and ordering temperatures of 5.1(2) K and 3.8(2) K for (5CAP)$_2$CuBr$_4$ and (5MAP)$_2$CuBr$_4$, respectively. High-field magnetization experiments on both compounds show upward curvature of $M(H,T)$. Magnetization measurements made at $T=1.3$ K show saturation occurs in (5MAP)$_2$CuBr$_4$ at 18.8 T and in (5CAP)$_2$CuBr$_4$ at 24.1 T. The magnetization curves are consistent with recent theoretical predictions. Single-crystal magnetization measured at 2.0 K indicates a spin-flop transition at 0.38 T and 0.63 T for (5CAP)$_2$CuBr$_4$ and (5MAP)$_2$CuBr$_4$, respectively.

DOI: 10.1103/PhysRevB.65.144412 PACS number(s): 75.40.Gb, 75.40.Cx, 75.50.Ee, 61.10.Nz

I. INTRODUCTION

For over two and a half decades, low-dimensional magnetism has played an integral role in the understanding of phase transitions and critical phenomena. During the past dozen years, there has been enhanced interest in low-dimensional magnetism in the condensed-matter physics community due to the discovery of the copper-oxide superconductors which contain layers of $S=\frac{1}{2}$, Cu(II) ions. Experimental investigations of the insulating parent compounds of the superconductors, such as La_2CuO_4, have demonstrated the existence of strong antiferromagnetic intraplanar interactions ($J\approx 1000$ K), with very weak interactions in the third dimension.[1] It has been proposed that the formation of Cooper pairs in the doped systems can be understood in terms of the antiferromagnetic interactions within the layers.[2] The consequent desire to understand the magnetic properties of the two-dimensional (2D) $S=\frac{1}{2}$ (or quantum) Heisenberg antiferromagnet (2D QHAF) has led to a large amount of theoretical[3] and experimental research.

The current physical realizations of the 2D QHAF are inappropriate for examination of a number of important theoretical predictions, particularly those involving field-dependent properties and higher relative temperatures, $T/J \geqslant 1$. The large exchange strengths in the copper oxides will require magnetic fields exceeding 1500 T to bring the magnetic moments of the copper ions to saturation. For this reason, to our best knowledge, no theoretical studies of the in-field properties of the 2D QHAF appeared until very recently.[4–6] The few previously known nonoxide examples of 2D QHAF's are characterized by much smaller exchange interactions but still have their own sets of limitations. Until more appropriate materials are available, a deeper understanding of the nature and properties of the 2D QHAF must be postponed.

Our research group endeavors to expand the available catalog of low-dimensional quantum antiferromagnets through the application of the principles of molecular-based magnetism.[7] We report here on a family of 2D QHAF's with relatively small intralayer exchange constants, permitting high-field studies. In this paper we present experimental investigations of low-temperature magnetization curves for 2D QHAF's. We report the synthesis and structure of (5CAP)$_2$CuBr$_4$ (5CAP=2-amino-5-chloropyridinium) and the magnetic properties of both (5CAP)$_2$CuBr$_4$ and (5MAP)$_2$CuBr$_4$ (5MAP=2-amino-5-methylpyridinium), two members of a family of insulating 2D $S=\frac{1}{2}$ Heisenberg antiferromagnets. This family has the general chemical formula A_2CuX_4, where A=5CAP or 5MAP and X=Br or Cl. The copper ion is in a 2^+ oxidation state with a d^9-electron configuration, producing one unpaired spin ($S=\frac{1}{2}$) and nearly quenched orbital angular momentum ($\langle g\rangle \approx 2.1$). The (5MAP)$_2CuX_4$ compounds were, to our best knowledge, the first to be synthesized in this family.[8,9] The (5CAP)$_2$CuX_4 compounds have been synthesized with the goals of reducing the number of protons in the cation for neutron-scattering experiments and with the intent of increasing the interaction strength. Expressing the Hamiltonian as

$$H = J\sum_{\langle ij\rangle} \vec{S}_i \cdot \vec{S}_j , \tag{1}$$

these materials have been found to have exchange strengths between 6 and 10 K, making it convenient to investigate their properties over a broad range of relative temperatures and applied fields. They are also easily prepared as single crystals.

TABLE I. Crystal data and structure refinement for $(5CAP)_2CuBr_4$.

Space group $C2/c$	Formula weight 642.32
$a=13.050(5)$ Å	$T=-130(2)$ °C
$b=8.769(3)$ Å	$\lambda=0.710\,73$ Å
$c=15.810(5)$ Å	$\rho_{Cal}=2.365$ g cm^{-3}
$\beta=94.31(3)°$	$\mu=10.362$ mm^{-1}
	Transmission coefficient = 0.124 31–0.478 08
$V=1804.1(11)$ Å^3	$R(F_0)=0.0476$ (=0.0679, all reflections)
$Z=4$	$R_w(F_0)=0.1053$ (=0.1153, all reflections)

II. EXPERIMENT

A. Synthesis and characterization

Crystals of $(5CAP)_2CuBr_4$ were prepared by slow evaporation of an aqueous solution of anhydrous copper(II) bromide (2.23 g, 10 mmol), dilute (20%) hydrobromic acid (8.1 g, 20 mmol), and 2-amino-5-chloropyridine (2.57 g, 20 mmol). The reaction is shown below.

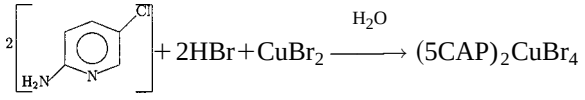

Although no attempt has been made to maximize yield, the net mass of harvested crystals is typically 50%–70% of the theoretical yield. Crystals as large as 650 mg have been grown. The crystals are a very deep maroon color, and for sizes larger than a few milligrams, appear black. The combustion analysis agrees with theoretical calculations. Analysis for $(C_5H_6N_2Cl)_2CuBr_4$, calculated(%), C, 18.73; N, 8.74; H, 1.89, found (%) C, 18.64; N, 8.47; H, 1.82. The infrared (IR) spectrum has the following principle bands: IR (KBr) ν (cm^{-1}): 3424 *m*, 3307 *m*, 1662 *s*, 1608 *s*, 1331 *m*, 820 *m*, and 661 *m*. The letters *s* and *m* indicate strong and medium intensities. Crystals of $(5MAP)_2CuBr_4$ were prepared by the method described above with the substitution of 2-amino-5-methylpyridine (2.22 g, 20 mmol) for the 2-amino-5-chloropyridine.

B. X-ray data collection

The x-ray-diffraction data for $(5CAP)_2CuBr_4$ were collected at -130 °C using a Siemens P4 diffractometer. The crystal data and structure refinement parameters are shown in Table I. Optimization of the orientation matrix and lattice parameters was done using least-squares calculation on 16 reflections in the range $4.64° < \theta < 12.23°$. Standard reflections (3) were monitored every 97 reflections to measure variations. The standard reflections varied by only 7.6%. A total of 3173 reflections were measured using an ω scan. Upon data reduction, 1598 unique reflections remained with 1181 having the criterion $|F| > 2\sigma$. Details of the crystal structure and data-collection method of $(5MAP)_2CuBr_4$ are given in the work of Place and Willett.[8]

C. Magnetic measurements

The measurements of susceptibility and low-field magnetization for single-crystal samples of $(5CAP)_2CuBr_4$ and $(5MAP)_2CuBr_4$ were made using a Quantum Design superconducting quantum interference device (SQUID) magnetometer. Initial single-crystal studies were hampered by the single-crystal samples shattering as a result of thermal cycling. This problem was overcome by embedding them in Emerson and Cummings Stycast 1266 epoxy. The orientation of the crystals was established by correlation of crystal morphology to x-ray structure. This correlation was verified by room-temperature electron paramagnetic resonance (EPR) on several single-crystal samples. The determination of the relation between the magnetic axes relative to crystal morphology was accomplished by observing the g values as a function of angle for three orthogonal rotations of the crystal. The powder and single-crystal susceptibility data for the two compounds were measured in fields up to 3 T using a SQUID. Corrections have been made for temperature-independent paramagnetism (TIP) (TIP$=60\times10^{-6}$ cm^3/mol) and the intrinsic diamagnetism (DIA) (DIA$=-329\times10^{-6}$ cm^3/mol for 5MAP and -280×10^{-6} cm^2/mol for 5CAP) of the samples. High-field magnetization data were collected for powder samples using a vibrating-sample magnetometer at the National High Field Magnet Laboratory in Tallahassee, Florida. Fields up to 30 T were applied to the samples at various temperatures. The EPR data, including single-crystal alignment, were collected on a Bruker EMX spectrometer operating at 9.3 GHz. Low-temperature EPR data were collected using an Oxford ESR-910 helium flow cryostat.

III. RESULTS

A. Crystal structure

Crystals of $(5CAP)_2CuBr_4$ are monoclinic in the space group $C2/c$, with $a=13.050(5)$ Å, $b=8.769(3)$ Å, $c=15.810(5)$ Å, and $\beta=94.31(3)°$. The atomic coordinates and equivalent isotropic displacement parameters are given in Table II. Selected bond distances and angles are presented in Table III. The structure of the molecular unit is shown in Fig. 1. Within the unit cell, the copper tetrabromide dianions sit at the edges and centers of planes parallel to the ab plane ($c=0.25$, 0.75), related by unit-cell translations and C centering, respectively (Fig. 2). These copper tetrahedra are flattened with the mean Br-Cu-Br large angle $\overline{\theta}\approx137°$. The copper ions lie on the twofold-symmetry axes. Consequently, each tetrahedra has its compression axis parallel to the b axis, eliminating any canting of the local g tensor. Equivalent

TABLE II. Atomic coordinates ($\times 10^4$) and equivalent isotropic displacement parameters ($Å^2 \times 10^3$) for $(5CAP)_2CuBr_4$. $U(EC)$ is defined as one-third of the trace of the orthogonality U_{ij} tensor.

	x	y	z	$U(EC)$
Br(1)	1368(1)	886(1)	3468(1)	21(1)
Br(2)	-1042(1)	-1079(1)	3512(1)	22(1)
Cu	0000	47(1)	2500	17(1)
Cl	751(2)	-4116(3)	6704(1)	32(1)
N(1)	1269(5)	-2430(7)	4476(4)	21(1)
C(1)	1607(6)	-3618(8)	4016(5)	17(2)
C(2)	1653(6)	-5069(8)	4412(5)	20(2)
N(2)	1882(5)	-3359(7)	3230(4)	26(2)
C(3)	1383(6)	-5210(8)	5222(5)	20(2)
C(4)	1063(5)	-3941(9)	5660(5)	20(2)
C(5)	983(6)	-2573(8)	5281(5)	19(2)

layers of $CuBr_4^{2-}$ tetrahedra are located one-half unit cell apart along the c axis. Each copper site is related to one in the adjacent layers by the c-glide symmetry operation.

The copper tetrahedra are tightly packed along the diagonals of the ab layers, with the separation between nearest-neighbor copper(II) ions in this direction being 7.86 Å. Such pairs of copper atoms are related by the C-centering operation. The Br···Br separation between adjacent tetrahedra along the diagonal is only 4.35 Å, approximately twice the radius of the bromide ion. The dihedral angle formed by the Cu-Br···Br-Cu pathway is approximately 22°. Such halide-halide contacts are known to create weak antiferromagnetic interactions,[9,10] which decrease rapidly with increased Br···Br separation. The Br···Br contact distances along the a and b axes are more than 10 Å and 7 Å, respectively, so the intralayer magnetic interactions must take place between copper ions related by C centering. Since each copper ion has four such identical neighbors, this lattice is *magnetically* equivalent to a square 2D lattice.

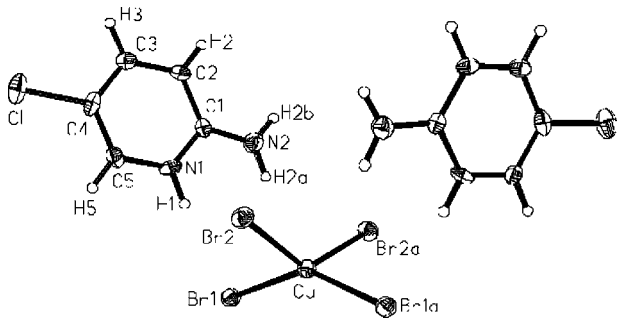

FIG. 1. Molecular unit of $(5CAP)_2CuBr_4$.

The layers of copper-bromide tetrahedra are stabilized into a 3D array by the organic cations which lie between the $CuBr_4^{2-}$ layers. They are stacked parallel to the ab diagonal and separated by 3.4 Å. Successive pyridinium rings within the stack are related by a twofold rotation. Looking down the stacking axis, the pyridinium substituent which points up along the c axis alternates between the 2-amino and the 5-chloro (see Fig. 3). The planes of the pyridine rings are tilted approximately 70° with respect to the copper planes, resulting in a separation of copper centers in neighboring planes of 7.88 Å. Weak hydrogen bonding between the pyridinium hydrogen (H1) and Br1 (refer to Fig. 1, $d_{H1-Br1} = 3.32$ Å) helps stabilize the structure. Very weak hydrogen bonding may also occur between the amino hydrogens ($H2a$, $H2b$) and two neighboring bromines from different tetrahedra ($d_{N2-Br2,Br2a} = 3.51$, 3.61 Å).

The magnetic layers are coupled in the third dimension by an interlayer interaction J' that occurs through Br···Br contacts along the c axis (Fig. 3). Copper sites along the c axis are related by two identical Br···Br contacts at a distance of 4.83 Å, with a dihedral angle of approximately 21°. The extra 0.48-Å separation in the intralayer Br···Br contact distances will lead to a significant reduction in the J'/J ratio.

$(5MAP)_2CuBr_4$ (Ref. 8) is isostructural with $(5CAP)_2CuBr_4$. The room-temperature lattice parameters for

TABLE III. Selected bond distances (Angstrom) and angles (degrees) for $(5CAP)_2CuBr_4$.

Bond distances (Å)			
Br(1)-Cu	2.3792(12)	Br(2)-Cu	2.3897(11)
Cl-C(4)	1.738(8)	N(1)-C(5)	1.359(10)
N(1)-C(1)	1.362(9)	C(1)-N(2)	1.338(10)
C(1)-C(2)	1.417(10)	C(2)-C(3)	1.360(11)
C(3)-C(4)	1.390(10)	C(4)-C(5)	1.342(11)
Bond angles (degrees)			
Br(1)′-Cu-Br(1)	143.95(7)	Br(1)-Cu-Br(2)	97.71(4)
Br(1)-Cu-Br(2)′	96.97(4)	Br(2)′-Cu-Br(2)	131.20(7)
C(5)-N(1)-C(1)	123.5(6)	N(2)-C(1)-N(1)	119.1(7)
N(2)-C(1)-C(2)	123.8(7)	N(1)-C(1)-C(2)	117.1(6)
C(3)-C(2)-C(1)	119.5(7)	C(2)-C(3)-C(4)	120.3(7)
C(5)-C(4)-C(3)	120.7(7)	C(5)-C(4)-Cl	119.1(6)
C(3)-C(4)-Cl	120.2(6)	C(4)-C(5)-N(1)	118.9(7)

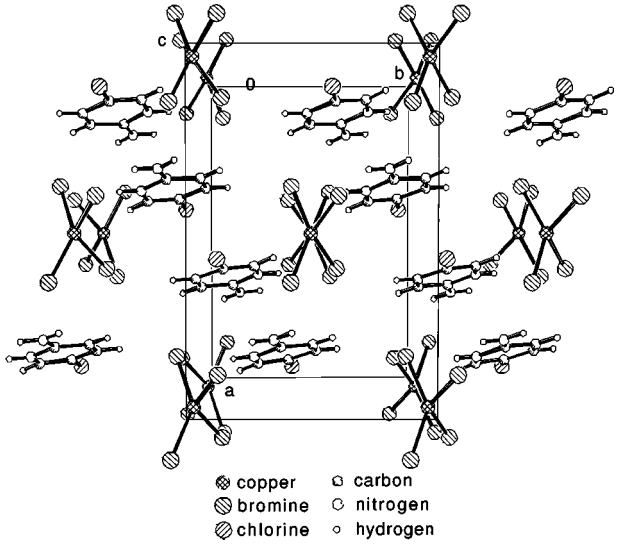

FIG. 2. View down c axis of $(5CAP)_2CuBr_4$ showing two adjacent C-centered $CuBr_4^{2-}$ planes in their eclipsed configuration.

$(5MAP)_2CuBr_4$ are $a=13.715(2)$ Å, $b=8.7162(2)$ Å, $c=16.013(4)$ Å, and $\beta=93.79(2)°$, reflecting its slightly larger unit cell. The intraplanar Br···Br distance is 4.54 Å, which is significantly longer than the corresponding value in $(5CAP)_2CuBr_4$ of 4.35 Å. The separation between the layers is also significantly enhanced due to the bulk of the methyl substituent resulting in a separation of 4.97 Å.

B. Powder susceptibility

The molar magnetic susceptibility (χ_m) as a function of temperature for a powder of $(5CAP)_2CuBr_4$ is shown in Fig. 4. A broad maximum is observed with the maximum value in χ_m (18.3×10^{-3} cm^3/mol) occurring near 8.0 K. The data

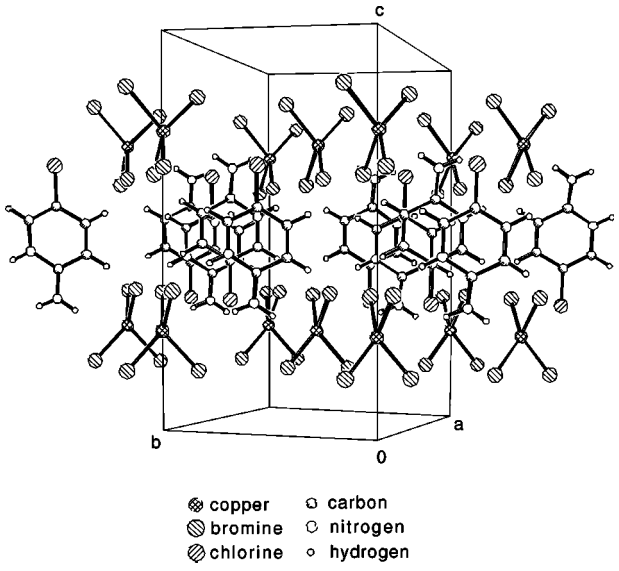

FIG. 3. View down the a axis of $(5CAP)_2CuBr_4$ showing the cross section of the planes and the orientation of the organic groups. The dashed lines mark the two sets of interplanar Br···Br contacts which cause the interplanar exchange J'.

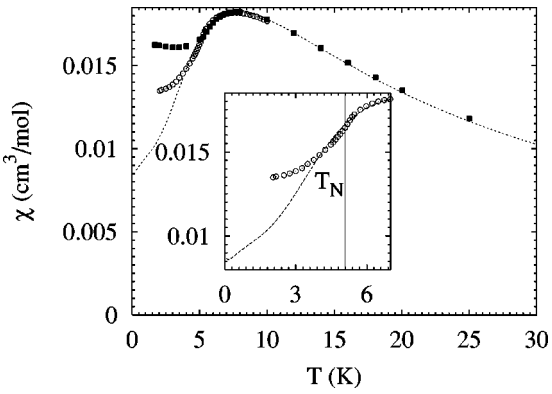

FIG. 4. χ_m vs T for $(5CAP)_2CuBr_4$. The dashed line is the 2D QHAF model using the parameters $J=8.5(2)$ K and $g=2.11(2)$. The data, marked as open circles, were collected at $H=0.1$ T and that marked as filled boxes were collected at $H=1.0$ T. The vertical line in the inset marks the ordering temperature of 5.08 K as determined by specific-heat measurements (Ref. 11).

have been compared to the theoretical predictions and simulation for the susceptibility of the 2D QHAF (described in Sec. IV). The dashed line shown in Fig. 4 represents a curve fit to the data resulting in an exchange interaction strength $J=8.5(2)$ K and $g_{ave}=2.11(2)$. This value of g_{ave} is in good agreement with powder and single-crystal room-temperature EPR measurements. The magnetic-susceptibility fitting procedure included only data at temperatures greater than 5.2 K, since the specific-heat studies[11] of $(5CAP)_2CuBr_4$ show the existence of an ordering transition at $T_N=5.08$ K. The dashed line shows the model expression for the ideal 2D QHAF with the same parameters extended down to $T=0$. The low-field powder susceptibility shows no anomaly at the ordering transition, but does break away from the model curve at a temperature very close to T_N. The data collected in a field above the spin-flop transition (Sec. IIII E below), shows a much stronger deviation from the model curve at T_N.

The data for $(5MAP)_2CuBr_4$ are shown in Fig. 5. The susceptibility of $(5MAP)_2CuBr_4$ is qualitatively identical to that of $(5CAP)_2CuBr_4$, with a slightly lower temperature for the maximum susceptibility (≈6 K). Comparison of these data to the model curve yields an interaction strength of $J=6.5(2)$ K and $g_{ave}=2.07(2)$.

C. High-field magnetization

The magnetizations as a function of field at $T=1.3$ K for $(5CAP)_2CuBr_4$ and $(5MAP)_2CuBr_4$ are shown in Fig. 6(a) plotted on a normalized scale M/M_{sat} where M_{sat} were determined to be 5980 and 5880 emu/mol, respectively. To our knowledge, this is the first report of the full magnetization curve for any 2D QHAF. (A preliminary report has appeared elsewhere.[12]) Note the upward curvature present in both data sets. The saturation fields appear to be close to 19 T and 24 T, respectively. Although these estimates are crude, we do note that the ratio of saturation fields (19 T/24 T = 0.79) is quite close to the ratio of exchange strengths as determined by the susceptibility data (6.8 K/8.5 K = 0.80).

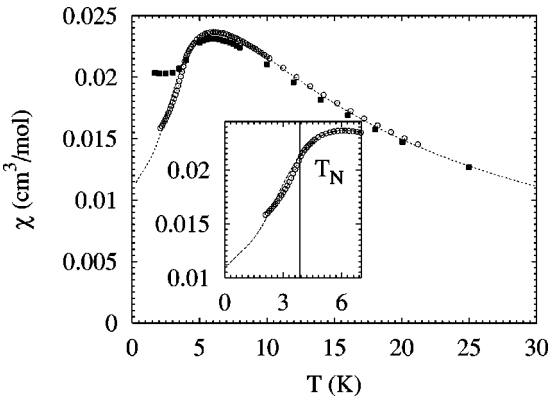

FIG. 5. χ_m vs T for $(5MAP)_2CuBr_4$. The dashed line is the 2D QHAF model using the parameters $J=6.5(2)$ K and $g=2.07(2)$. The data, marked as open circles, were collected at $H=0.1$ T and that marked as filled boxes were collected at $H=1.0$ T. The vertical line in the inset marks the ordering temperature of 3.8 K as determined by the deviation of the powder susceptibility data from the ideal 2D QHAF curve.

In Fig. 6(b), the data are plotted again on a normalized scale, M/M_{sat} versus H/H_{sat}, where H_{sat} is 18.8 T and 24.1 T for $(5MAP)_2CuBr_4$ and $(5CAP)_2CuBr_4$, respectively. These values of H_{sat} were determined from mean-field approximations using the interaction strengths, J, as determined from the powder susceptibility data for each compound. Details for this procedure are described in Sec. IV. Included in Fig. 6 are results from numerical calculations of $M(H,T=0)$ for finite 1D (Ref. 13) and 2D (Refs. 4 and 5) Heisenberg systems, and Monte Carlo simulation at $T/J=0.2$.[14] The magnetization data of $(5MAP)_2CuBr_4$ is slightly higher than that of $(5CAP)_2CuBr_4$ until a point just below the saturation field.

The temperature dependence of the molar magnetization as a function of field for a powder sample of $(5MAP)_2CuBr_4$ is shown in Fig. 7. The data were collected at three different temperatures ($T=1.3$, 2.4, 4.4 K) corresponding to relative temperatures T/J of 0.19, 0.35, and 0.65, respectively. The data at 1.3 K and 2.4 K both exhibit upward curvature and saturate at approximately 20 T. The upward curvature is no longer present in the higher-temperature data.

D. Single-crystal susceptibility

Figure 8(a) shows the single-crystal magnetic-susceptibility data for $(5CAP)_2CuBr_4$ collected with the applied magnetic field both in and perpendicular to the 2D magnetic layer. The powder data as well as the 2D QHAF model curve are also included in this figure. Notice that at 5.1 K the data sets diverge from one another. This is an expected result for an isotropic 2D QHAF as it goes through dimensional crossover to an anisotropic 3D ordered state. In a 3D QHAF with an Ising anisotropy, the three distinct susceptibility curves are $\chi_\parallel$, dropping toward zero, $\chi_\perp$, staying at or close to χ_{max}, and the powder data, χ_{pow}, which should fall between the two previous curves ($\frac{2}{3}\chi_{max}$). Note that the onset of the three-dimensional behavior in the single-crystal data begins at a temperature (5.1 K) which is in excellent agreement with the critical temperature determined by specific-heat studies.[11] The $(5MAP)_2CuBr_4$ data shown in Fig. 8(b) exhibit the same dimensional crossover behavior. For the $(5MAP)_2CuBr_4$ data the onset of 3D order occurs at a lower temperature of 3.8 K. The single-crystal data for both compounds were collected with $H_{appl}=0.2$ T and include corrections for diamagnetic and temperature-independent

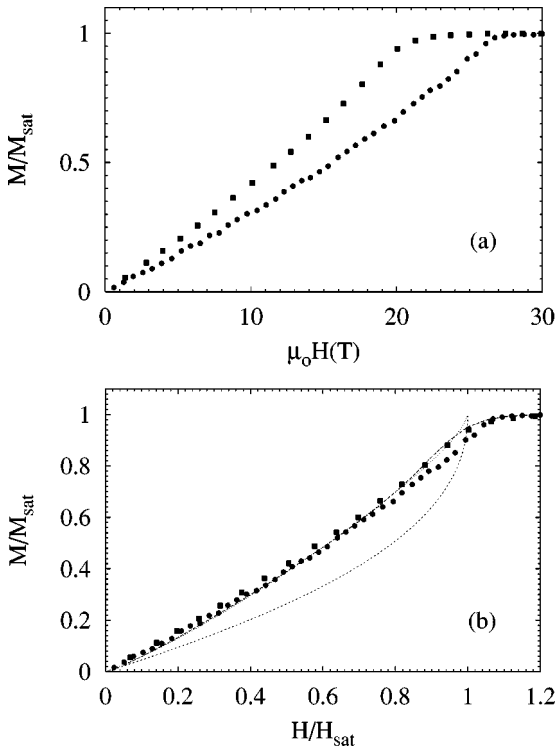

FIG. 6. (a) Relative molar magnetization vs $H(T)$ at $T=1.3$ K for powder samples of $(5MAP)_2CuBr_4$: filled circles, $(5CAP)_2CuBr_4$: filled boxes. (b) Same data as in (a) but plotted on a normalized field scale, H/H_{sat}. $H_{sat}=18.8$ T for $(5MAP)_2CuBr_4$, $H_{sat}=24.1$ T for $(5CAP)_2CuBr_4$. The dotted line is a result of 2D numerical calculations at $T=0$ K, the long-dashed line is the result of Monte Carlo simulations at $T/J=0.2$, and the dashed line is the result of 1D numerical calculations at $T=0$ K.

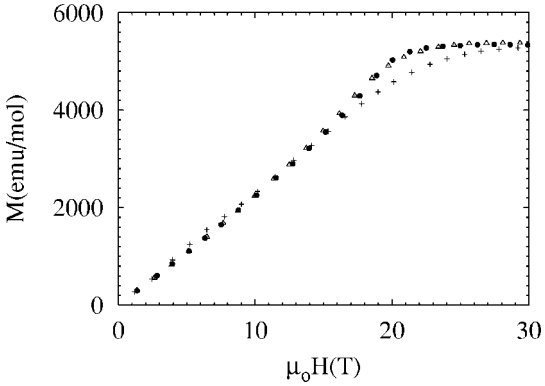

FIG. 7. Molar magnetization vs $H(T)$ at three different temperatures for a powder sample of $(5MAP)_2CuBr_4$. $T=1.3$ K (filled circles), $T=2.4$ K (triangles), and $T=4.4$ K (crosses).

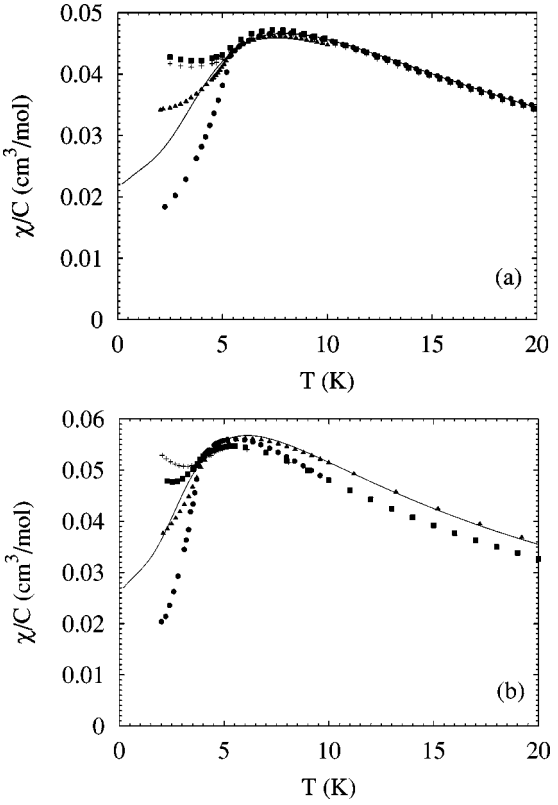

FIG. 8. Single-crystal χ/C versus temperature at $H=0.2$ T. (a) $(5CAP)_2CuBr_4$, (b) $(5MAP)_2CuBr_4$. $\chi_\perp$: filled boxes, H applied $\|$ to b, triangles, H applied $\|$ to c, $\chi_\|$: filled circles, H applied $\|$ to a, and χ_{pow}: crosses, $H=0.1$ T. Solid line represents 2D QHAF model.

paramagnetic contributions. Note that the data in Figs. 8(a) and 8(b) have been scaled by the Curie constant for a spin-$\frac{1}{2}$ system, $C=0.375(g/2)^2$, where the g value is g_a, $g_b=g_c$, or g_{pow} depending upon the data set.

E. Single-crystal magnetization

Figure 9(b) shows single-crystal magnetization for $(5MAP)_2CuBr_4$ at $T=2.1$ K with magnetic field applied in three orthogonal directions. Clearly visible in Fig. 9(b) is a change in slope of the magnetization data when the magnetic field is applied parallel to the crystallographic a axis. The change of slope in the magnetization data occurs at $H_{appl}=0.63$ T. The inflection is only observed when the field is applied along the a axis and is not found when the field is applied along the b or c^*, as seen in the other two data sets displayed in Fig. 9(b). The $(5CAP)_2CuBr_4$ single-crystal magnetization curve also at $T=2.1$ K, in Fig. 9(a), also shows a change in slope at $H_{appl}=0.30$ T when H_{appl} is along the a axis. In the case of $(5CAP)_2CuBr_4$ data shown in Fig. 9(a), the transition is less pronounced and even appears in one of the perpendicular curves. This is due to difficulties of aligning the $(5CAP)_2CuBr_4$ crystal in the applied field. Slight misalignment results in a mixing of the features of orthogonal magnetization curves.

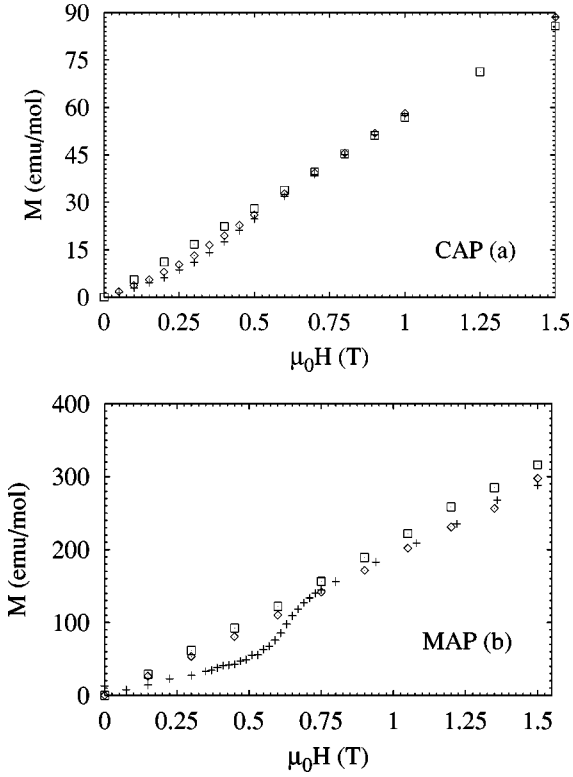

FIG. 9. Single-crystal molar magnetization at $T=2.1$ K. (a) $(5CAP)_2CuBr_4$: crosses, H applied $\|$ a, diamonds, H applied $\|$ b, and open boxes, H applied $\|$ c. (b) $(5MAP)_2CuBr_4$: crosses, H applied $\|$ a, diamonds, H applied $\|$ b, and open boxes, H applied $\|$ c.

F. EPR

The angular dependence of the single-crystal data for three orthogonal rotations in the ab, bc^*, and ac^* planes, respectively, is found in Fig. 10. In the case of $(5CAP)_2CuBr_4$, Fig. 10(a), the angular study clearly shows two principle g values: $g_b=2.22$ and $g_a=g_{c*}=2.06$. Powder simulation for $(5CAP)_2CuBr_4$ yields two g values, $g_\perp=2.22$ and $g_{||}=2.06$. The Jahn-Teller compression of the copper's tetrahedral environment along the b axis is the cause of the 7.2% difference between g values along the different axes. The same is true for $(5MAP)_2CuBr_4$, as seen in Fig. 10(b). Here $g_b=2.24$ while $g_a=g_{c*}=2.05$. This is in agreement with the powder simulation values, $g_\perp=2.23$ and $g_{||}=2.06$, yielding a difference of 7.6% for this compound.

The room-temperature X-band powder EPR spectra display evidence of a slightly anisotropic copper signal for each compound. For $(5MAP)_2CuBr_4$, the single-crystal average g value is $\langle g_{sc}\rangle=\sqrt{\frac{1}{3}(g_x^2+g_y^2+g_z^2)}=2.12$. The average g value as determined by a comparison of powder EPR data to powder simulation, using Bruker's EPR simulation package SIMFONA, is $\langle g_{sim}\rangle=2.12$. The corresponding $(5CAP)_2CuBr_4$ g values are $\langle g_{sc}\rangle=2.11$ and $\langle g_{sim}\rangle=2.11$.[15]

The low-temperature signals for the X band are quite remarkable. Figures 11(a) and 11(b) show room-temperature powder data as the top spectra, and low-temperature spectra, $T=3.2$ K, are in the bottom half of the figures. The

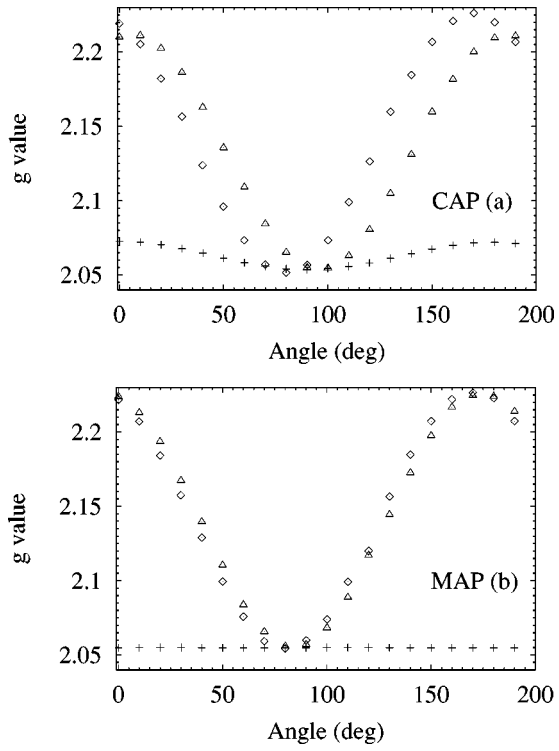

FIG. 10. Single-crystal, room-temperature, *X*-band EPR for $(5CAP)_2CuBr_4$ in (a) and $(5MAP)_2CuBr_4$ in (b). In both cases the crosses represent data for rotations in the ab plane about the c^* axis while triangles are for rotations in the ac^* plane and diamonds are for rotations in the bc^* plane.

$(5CAP)_2CuBr_4$ data are on the right and $(5MAP)_2CuBr_4$ data are on the left. The rich and complex spectra observed in the *X*-band data in the lower half of Fig. 11 are not found in the *Q*-band spectra.

IV. DISCUSSION

A. Structure

The crystal structures of the compounds in the $(5CAP/5MAP)_2CuBr_4$ family show that the copper ions lie on a *C*-centered lattice, with four equivalent nearest neighbors parallel to the ab plane (Fig. 2). The $Br\cdots Br$ contacts between $CuBr_4^{2-}$ tetrahedra along the diagonals lead to antiferromagnetic interactions of a few Kelvin, consistent with the values observed for other structures in which copper tetrabromide anions are in contact.[9,10] The distances to the next-nearest neighbors within the planes are much greater, with negligible $Br\cdots Br$ ion contacts. The magnetic interactions between next-nearest neighbors (J_{nnn}) can therefore be ignored. The equivalence of all nearest-neighbor interactions, caused by the *C* centering, plus the absence of J_{nnn}, permits the magnetic layers to be considered as a square magnetic lattice despite the absence of fourfold symmetry.

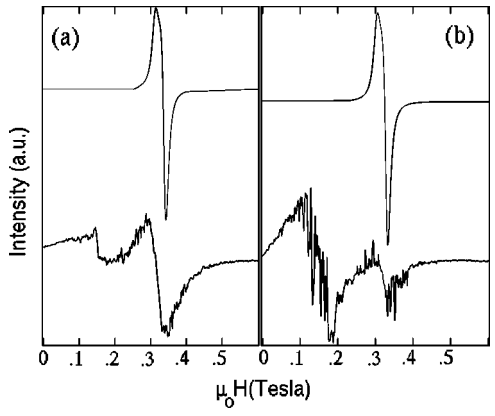

FIG. 11. Powder *X*-band EPR for $(5MAP)_2CuBr_4$ (a) and $(5CAP)_2CuBr_4$ (b). The top spectra are at room temperature and the bottom spectra were collected on an Oxford ESR910 He cryostat at 3.2 K.

The strength of the intraplanar interaction is predominantly dependent upon the value of the $Br\cdots Br$ contacts. This is evidenced by the change in interaction strength going from $(5MAP)_2CuBr_4$ to $(5CAP)_2CuBr_4$. The substituent in the five position on the pyridine ring protrudes into the copper tetrahedra layer (Fig. 3). The larger methyl group forces the tetrahedra farther apart, increasing the $Br\cdots Br$ contact distance between adjacent tetrahedra from 4.35 Å for $(5CAP)_2CuBr_4$ to 4.54 Å for $(5MAP)_2CuBr_4$ and causing the decrease in the magnitude of the exchange interaction from 8.5 K for $(5CAP)_2CuBr_4$ to 6.8 K for $(5MAP)_2CuBr_4$. Such sensitivity of the structure to the size of the five substituent provides some adjustability in the magnetism of these systems, always a desirable goal of magnetochemistry.

Studies have also been carried out on the chloride analogs to these systems [$(5CAP)_2CuCl_4$ and $(5MAP)_2CuCl_4$].[16] The van der Waal's radius of a chloride ion is smaller than that of a bromide ion, whereas the unit-cell constants of $(5CAP)_2CuCl_4$ and $(5MAP)_2CuCl_4$ are nearly the same as the bromide complexes. Therefore, the absolute overlap of the $Cl\cdots Cl$ wave functions between neighboring tetrahedra is considerably less than that of the $Br\cdots Br$ overlap. The smaller van der Waal's radius of the chloride ion produces a weaker exchange between the copper centers (1.14 K and 0.76 K, respectively).

B. Susceptibility

The susceptibility of the 2D QHAF was originally calculated by Rushbrooke *et al.* using high-temperature series expansions (HTSE).[17] This procedure predicted a broad maximum in χ_m at $T_{max}\approx J$ but was invalid for temperatures below T_{max}. The discovery of high-temperature superconductivity in 1986 stimulated renewed interest in the 2D QHAF model and more extensive studies have been done. The techniques used to evaluate the susceptibility include spin-wave expansions[18] about $T=0$, Padé approximant extensions to the results of HTSE,[19] and quantum Monte Carlo calculations.[21,20] The low-temperature susceptibility is predicted[18,20] to approach the limiting value in a linear manner,

$$\frac{\chi_m J}{C}=\frac{\chi_0 J}{C}+\frac{0.15\,616T}{J}, \tag{2}$$

where $\chi_0 J/C=0.174$. There is no evidence of unusual quantum behavior in the susceptibility as $T\rightarrow 0$, as has been re-

cently demonstrated to be the case for the 1D QHAF.[22] The maximum susceptibility has been shown to have a value of $\chi_{max}=0.375(1)C/J$ at a temperature $T_{max}=0.936$ J.[18] The ratio of the two limiting susceptibilities $\chi_0/\chi_{max}=0.416$.

For the purposes of data analysis, the theoretical results were fit to an empirical expression for the susceptibility

$$\chi_m=\frac{0.375g^2}{4T}\sum_{n=1}^{5}\frac{a_nK^n}{b_nK^n}, \tag{3}$$

where $K=J/T$. The coefficients a_n and b_n, listed in Table IV, were determined using a standard nonlinear, least-squares-fitting algorithm. This functional form can be used to determine the J and g values from magnetic-susceptibility data for any 2D QHAF. This functional form accurately describes the predicted susceptibility of the 2D QHAF for a range of $0.15<T/J$.

The powder susceptibilities of $(5CAP)_2CuBr_4$, Fig. 4, and $(5MAP)_2CuBr_4$, Fig. 5, are well described by this empirical expression for the 2D QHAF with the exchange strengths 8.5(2) K and 6.5(2) K, respectively. The best fits are shown as the dashed lines in Figs. 4 and 5. The model curves based on these parameters (J and g) have been extended to zero temperature (dashed lines) and it is noted that the experimental data break away from the theoretical curves at temperatures near 5.1(2) K for $(5CAP)_2CuBr_4$ and 3.8(2) K for $(5MAP)_2CuBr_4$. Since the T_N of $(5CAP)_2CuBr_4$ is known to be 5.08 K by specific-heat measurements,[11] we can establish a close agreement between T_N and the temperature of divergence between the experimental data and the theoretical prediction. On the basis of this comparison, we estimate the Néel temperature of $(5MAP)_2CuBr_4$ to be 3.8(2) K.

Initially all of the powder susceptibility data were collected at 1 T, well above the field-induced transition observed in the single-crystal magnetization data. This caused the powder data to deviate sharply from the 2D QHAF curve below T_N, being dominated by the $\chi_\perp$ behavior. When collected in a field smaller than the spin-flop field, the data still noticeably deviate from the model curve, but now approach a value consistent with the mean-field-theory estimates of a 3D QHAF with a weak Ising anisotropy. The powder susceptibilities in the ordered states approach constant values near 0.012 cm^3/mol and 0.014 cm^3/mol for the $(5CAP)_2CuBr_4$ and $(5MAP)_2CuBr_4$, respectively. These are near the theoretical limiting values of $\frac{2}{3}\chi_\perp$, taken from the single-crystal data, of 0.011 cm^3/mol and 0.014 cm^3/mol, respectively.

The single-crystal susceptibilities for both of the compounds clearly show dimensional crossover from isotropic 2D behavior to anisotropic 3D behavior by the appearance of $\chi_\perp$ and $\chi_{||}$ susceptibilities. In $(5CAP)_2CuBr_4$, the onset of 3D order occurs at a temperature of 5.1 K as depicted in Fig. 8(a). In the $(5MAP)_2CuBr_4$ the onset of 3D order begins at 3.8 K and again is marked by the separation of the parallel and perpendicular susceptibilities as shown in Fig. 8(b).

Analysis of the single-crystal susceptibility data shows that there is an internal anisotropy axis which lies along the crystallographic a axis for each compound. The $(5CAP)_2CuBr_4$ and $(5MAP)_2CuBr_4$ $\chi_\parallel$ data shown in Figs. 8(a) and 8(b), respectively, appear to fall well below the $\chi_\perp$ but do not quite extrapolate to $\chi_\parallel(0)=0$ which is what is expected of a true 3D QHAF with an Ising anisotropy. The failure of the data to extrapolate to zero may be due to either a misalignment of the sample in the applied field or to spin canting within the ordered state. From the extrapolated value of $\chi_\parallel(0)$ the amount by which the sample is misaligned can be estimated. The misalignment of the 5MAP sample would have to be about 5° and in the 5CAP about 20°. The method by which the samples were aligned in the field allows for an error of at least 5°, easily explaining the problems with the 5MAP data. An alignment error of 20° in the 5CAP data is still not outside the realm of possibilities, when one considers that in the case of 5CAP the a and b axes do not lie directly along sample diagonals as was the case for 5MAP. Also, there is an angle of 5° between c and c^* and 4° in the 5MAP. While spin canting would explain a nonzero value of $\chi_\parallel(0)$, structural considerations tend to rule this out as an option. Each copper atom is related to the next by the C centering in the lattice thus removing any possibility that any two copper sites would experience different chemical environments. It is possible that there is a structural phase change as a function of temperature which would remove this symmetry, but no anomalies were observed in the specific-heat study[11] of 5CAP except at T_N. To conclusively determine whether spin canting exists in the 5CAP and 5MAP systems, a determination of the magnetic lattice by neutron scattering will have to be made.

Anisotropy in the $CuBr_4^{2-}$ complexes is due to distortions of the coordination about the copper site from pure tetrahedral symmetry. In 5CAP and 5MAP, the distortions consist of a compression along the b axis which is reflected in the g-tensor anisotropy: $g_\parallel=g_b$ and $g_\perp=g_a=g_c$. Surprisingly, the unique magnetic axis, as determined by $\chi_\parallel$, is not the same as the principle axis of the g tensor.

Previous work by Willett[23] has shown that for magnetic copper-chloride compounds the easy axis lies along the unique axis of the coordination sphere of the copper-chloride tetrahedra, but in the case of the copper-bromide compounds the easy ($\chi_\parallel$) axis tends to lie perpendicular to the compression axis. Willett attributed this to a reversal in the sign of the spin-orbit coupling parameters from the chloride to the bromide compounds. Given that the b axis is the bromide compression axis, the magnetic anisotropy axis is expected to lie along either the a or c^*. It is not currently clear why a is selected over c^*, but the explanation may be found in the difference of the dipolar energies of the two configurations.

C. Magnetization

The low value of the exchange strength found for these 2D QHAF compounds allows the antiferromagnetic interactions to be overcome by experimentally accessible magnetic fields. The required saturation fields can be estimated at $T=0$ K by a mean-field calculation. Assuming the critical field depends only on the exchange strength, the equation for an $S=\frac{1}{2}$ system is given by[24]

$$H_{sat}=\frac{zJ}{g\mu_\beta}, \tag{4}$$

TABLE IV. 2D QHAF model polynomial coefficients.

n	a_n	b_n
1	0.998 586	-1.842 79
2	-1.285 34	1.141 41
3	0.656 313	-0.704 192
4	0.235 862	-0.189 044
5	0.277 527	-0.277 545

where z is the number of nearest neighbors. Therefore at $T=0$ K, the predicted values of the saturation field for $(5MAP)_2CuBr_4$ and $(5CAP)_2CuBr_4$ are 18.8 T and 24.1 T, based upon the values for J obtained from the fits to the susceptibility data. The fact that $(5MAP)_2CuBr_4$ is observed to saturate at fields lower than $(5CAP)_2CuBr_4$ is consistent with the smaller exchange strength. These predicted saturation values are in good agreement with the experimental data shown in Figs. 6 and 7.

The values of M_{sat} for the high-field magnetization are in good agreement with the g values known from powder EPR. Given that

$$M_{sat}=g\mu_\beta NS \tag{5}$$

and using either the powder EPR g values (2.11 and 2.12) or the 2D QHAF model fit g values (2.10 and 2.07) the difference between the measured M_{sat} (5980 and 5880 emu/mol) and the calculated M_{sat} (5900 emu/mol and 5905 emu/mol) is on the order of 1% (1.37% and 0.45%).

A noteworthy feature in the field-dependent magnetization data contained in Figs. 6 and 7 is the upward curvature of the low-temperature magnetization data. This behavior is qualitatively similar to theoretical[13,24] and experimental[25] realizations of the $T=0$ K magnetization curve of the one-dimensional $S=1/2$ Heisenberg antiferromagnet, indicated by the dashed curve in Fig. 6. The theory for the 1D QHAF also predicts that for relative temperatures $kT/J<0.5$, the magnetization has positive curvature prior to saturation. However, it is clear that the curvature in the magnetization curve of the 1D model is more extreme than found experimentally for $(5CAP)_2CuBr_4$ and $(5MAP)_2CuBr_4$.

Calculations for the magnetization curve of the 2D QHAF have recently appeared.[4,5,14] These calculations have been based on a diagonalization of finite lattices at $T=0$ K,[4] a $T=0$ K spin-wave expansion with second-order corrections,[5] and quantum Monte Carlo studies on large systems at both zero and finite temperatures.[14] All three sets of predictions are in good agreement with each other at $T=0$ K, but the two more recent papers[5,14] contain more precise predictions. The $T=0$ K spin-wave expansion[5] is represented as the dotted line, the quantum Monte Carlo calculations[14] as the long-dashed line, and the 1D QHAF prediction[24] as a short-dashed line in Fig. 6(b), with the less precise data of Yang and Mütter[4] not shown. The field axis for the predictions was scaled by saturation fields based upon the experimental exchange strengths as determined by susceptibilities [Eq. (4)]. The data are in much better quantitative agreement with the 2D predictions than with the 1D predictions. We emphasize that the agreement between theory and experiment in Fig. 6(b) is *not* due to a fit, since no parameters were allowed to vary.

The agreement between the experimental data and theory is poorer for low fields, but becomes better as the saturation field is approached. We attribute the low-field discrepancies to a combination of the 3D ordering and finite temperature effects. In the 3D ordered state, the low-temperature ratio of M/H in fields above the spin-flop field are nearly double the values predicted for the ideal 2D QHAF susceptibility. The initial slope of the theoretical magnetization curve is derived from the isolated layer model, and for this reason the slope is consistently lower than the experimental magnetization data. As the field increases toward the saturation value, the weak 3D interactions become increasingly irrelevant and the data fall onto the theoretical curve.

At the highest fields, the effects of finite temperatures are observed. The $T=0$ K magnetization curve is predicted to have a weak logarithmic divergence at H_{sat} due to the quenching of quantum fluctuations,[5] but this feature is not observed because the high-field magnetization curve is rounded due to the presence of thermal excitations. The magnetization curve $M(H,T)$ has recently been calculated for several finite temperatures by quantum Monte Carlo techniques;[14] these results are presented in Fig. 6(b) as the long-dashed lines corresponding to the relative temperature $T/J=0.2$. The scaled temperatures for the $(5MAP)_2CuBr_4$ and $(5CAP)_2CuBr_4$ compounds are $T/J=0.19$ and 0.15, respectively.

Similar magnetization behavior has been observed experimentally[16] for the analogous chloride complexes, $(5CAP)_2CuCl_4$ and $(5MAP)_2CuCl_4$. The isostructural chloride compounds have significantly weaker exchange interactions because of the smaller Cl radius resulting in a diminished halide-halide overlap. The low-temperature magnetization curves for the chloride analogs are similar in shape to those observed for the bromides, but the saturation fields are considerably smaller (3.8 T and 2.4 T, respectively), which is consistent with the smaller exchange strengths (1.14 K and 0.76 K, respectively).

Low-field single-crystal magnetization data for $(5CAP)_2CuBr_4$ and $(5MAP)_2CuBr_4$ are presented in Fig. 9. The $(5MAP)_2CuBr_4$ magnetization data exhibit a definite change of slope at $H=0.63$ T, Fig. 9(b), when the applied field is parallel to the nominal easy axis. The same behavior is seen in the $(5CAP)_2CuBr_4$ data, Fig. 9(a), in which the change of slope appears at $H=0.38$ T when the field is applied parallel to the nominal easy axis. When the applied field is perpendicular to the easy axis, for both the $(5CAP)_2CuBr_4$ and $(5MAP)_2CuBr_4$, Fig. 9, the magnetization data are linear. These data sets were all collected at $T=2.1$ K, well below T_N for both compounds.

The change in slope exhibited by these magnetization data is evidence of a spin-flop[26] transition due to a weak internal anisotropy field, H_{aniso}. The strength of the anisotropy field relative to the primary exchange field can be determined by mean-field arguments[26] given the spin-flop field, H_{sf}, and the saturation magnetization field, H_{sat}:

$$H_{aniso} \approx \frac{H_{sf}^2}{2H_{sat}}. \quad (6)$$

Based on Eq. (6), the anisotropy fields for $(5CAP)_2CuBr_4$ and $(5MAP)_2CuBr_4$ are 0.0030 T and 0.0075 T, respectively. Arguments given below place the value of the 3D exchange at $J' \approx 0.08J$ for both compounds. When J' is compared to the anisotropy field, where $H_{aniso} \approx 0.0004 H_{ex}$, clearly J' is a stronger interaction. This implies that J' is the dominant interaction that drives the system from a 2D QHAF to a 3D QHAF with a weak Ising anisotropy.

D. Three-dimensional interactions

Ultimately, a transition to long-range order will occur for all two-dimensional Heisenberg antiferromagnets at low enough temperatures. This transition can be brought about either by the presence of small amounts of anisotropy (XY or Ising) or by magnetic interactions J' between the magnetic planes.[27] A useful parameter for characterizing low-dimensional magnetic systems is the ratio of the temperature at which long-range order occurs to the interaction energy, T_N/J. The properties of a number of 2D QHAF are compared in Table V where it is noted that even the best isolated[28] 2D QHAF's become 3D ordered when the T_N/J ratio has dropped to a value of $\geqslant 0.17$. Values between 0.2 and 0.4 have previously been found for other compounds which exhibit properties of 2D QHAF's.

The transition to long-range order in $(5CAP)_2CuBr_4$ has been previously determined by specific-heat studies.[11] The specific heat of this compound shows a sharp maximum at 5.08 K which has been attributed to a magnetic ordering transition. An analysis of the specific-heat data above T_c shows the compound's behavior to be that of a 2D QHAF with an exchange constant of 8.6 K, in excellent agreement with the value obtained from the powder magnetic-susceptibility studies. The ratio of T_c/J for $(5CAP)_2CuBr_4$ is therefore 0.60 (Table V). While this value is higher than those found for the other 2D QHAF's reported in Table V, we note that it is not high enough to prevent the observation of the characteristic rounded maximum in the magnetic susceptibility or of the characteristic upward curvature in the magnetization curve.

The powder magnetic-susceptibility data of $(5CAP)_2CuBr_4$ also show evidence of 3D ordering. The data are well described by the 2D QHAF model of the susceptibility at temperatures above T_N but deviate from the model curve at lower temperatures, Fig. 4, clearly defining the Néel transition. The powder susceptibility data collected in fields below the spin-flop field, $H = 0.1$ T, show only a small systematic deviation from the 2D model, first dropping below the model at T_N then curving up to cross it at lower temperatures as the data approach the powder average. The powder data collected in a field of 1.0 T, above the spin-flop field, show a more pronounced deviation from the 2D model at T_N. Assuming the same relation between the onset of 3D order and deviation of powder data from the 2D QHAF model, the critical temperature for $(5MAP)_2CuBr_4$ can be estimated from Fig. 5 to be 3.8(2) K which would correspond to a critical ratio of $T_N/J = 0.58$.

The specific-heat measurements[11] of $(5CAP)_2CuBr_4$ are more sensitive to the crossover from 2D QHAF behavior to the 3D ordered state than is the susceptibility data. The magnetic specific heat is clearly higher than the prediction for the 2D model with $J/k = 8.5$ K for temperatures as high as 6.5 K (Fig. 4 in Ref. 11), a full 30% above T_N.

A more sensitive indicator of the degree of isolation of the 2D layers is the value of the correlation length ξ at the critical ratio T_N/J. According to the theory of Chakravarty, Halperin, and Nelson,[29] the correlation length diverges exponentially at low temperatures, with only a weak temperature dependence in the prefactors.[30] The full expression for the correlation length is

$$\frac{\xi}{a} = \frac{e}{8}\frac{c/a}{2\pi\rho_s}\exp\left(\frac{2\pi\rho_s}{T}\right)\left[1 - 0.5\frac{T}{2\pi\rho_s} + O\left(\frac{T}{2\pi\rho_s}\right)^2\right], \quad (7)$$

where $c = 1.657Ja$ and $\rho_s = 0.1800J$ (Ref. 31) are the renormalized spin-wave velocity and spin-stiffness constants, respectively, and the correlation length is expressed in units of the lattice constant a. For 5CAP and 5MAP at their critical ratio $T_N/J = 0.60$, Eq. (7) predicts the correlation length to be $\xi/a = 2.2$. In comparison, the correlation length ratios (ξ/a) at T_N for $Sr_2CuO_2Cl_2$ and deuterated copper formate tetrahydrate have been determined by neutron-scattering experiments to be close to 220 (Ref. 28) and 55 (Ref. 32), respectively.

The large differences between the correlation lengths of the four compounds at the critical temperatures is a reflection of large differences in the relative ratios of interplanar to intraplanar exchange, J'/J. According to the mean-field theory of magnetic ordering in low-dimensional magnets,[33] long-range order will set in when the thermal energy is comparable to the interaction energy between blocks of correlated spins of the z neighboring layers,

$$kT_N \approx zJ'S(S+1)\left(\frac{\xi(T_N)}{a}\right)^2. \quad (8)$$

Using the value of 2.2 for ξ/a at T_N yields a value for $J'/k \approx 0.14T_N = 0.14\ (0.60J/K) = 0.08J/K = 0.72$ K. A similar value, $J'/k = 1.0$ K, was obtained by analysis of the spin-wave contribution to the magnetic specific heat in the ordered state.[11] We view the two estimates to be equivalent, considering the approximations used in the two analyses. The same ratio is found for 5MAP. In contrast, the same calculation for $Sr_2CuO_2Cl_2$ yields a J'/J ratio of 1.2×10^{-6}.

Why is the J'/J ratio so large in the 5CAP/5*MAP* family of 2D QHAF's? One important reason lies in the relationship between copper sites in two adjacent layers. For the well-isolated systems (La_2CuO_4, $Sr_2CuO_2Cl_2$, copper formate), adjacent layers are staggered, with the copper sites in one layer displaced by $(\frac{1}{2}, \frac{1}{2})$ with respect to those in adjacent layers, placing the metal ions equidistant from four equivalent metal sites in the layer above. Not only does this dis-

TABLE V. Examples of $S=\frac{1}{2}$ 2D Heisenberg antiferromagnets.

Compound	J/k (K)	T_N (K)	T_N/J	Comments	Reference
La_2CuO_4	≈ 1500	310	0.21	slight hidden canting	47, 48
$Sr_2CuO_2Cl_2$	≈ 1450	251	0.17	no canting	28
$Cu(COO)_2 \cdot 4H_2O$	70	16.5	0.24	CuF4H, canting	32, 35, and 49
$Cu(COO)_2 \cdot 2CO(NH_2)_2 \cdot 2H_2O$	70	15.5	0.23	CuFUH, canting	36
$CuF_2 \cdot 2H_20$	26	10.9	0.42	higher 3D interactions	37, 43
$[Cu(PyNO)_6][BF_4]_2$	4.4	0.62	0.28	structural transition	50
$K_2V_3O_8$	12.6	4.0	0.32	spin canting	51
$(5CAP)_2CuBr_4$	8.5	5.08	0.60	strong 3D interactions	this work, 11
$(5MAP)_2CuBr_4$	6.5	3.8	0.58	strong 3D interactions	this work
$(5CAP)_2CuCl_4$	1.14	0.74	0.64	strong 3D interactions	16
$(5MAP)_2CuCl_4$	0.76	0.44	0.57	strong 3D interactions	16

placement increase the interlayer Cu···Cu distance, it also provides a net cancellation of the four antiferromagnetic interactions from the adjacent layer. To first order J' vanishes in staggered systems, and 3D order is actually brought about by the presence of weak anisotropy terms (Ising, XY, Dzyaloshinsky-Moria) in the Hamiltonian.

In contrast, the copper layers of the 5CAP/5MAP family lie directly above adjacent layers (Fig. 2). Hence there is a much shorter interplanar Cu···Cu distance and no cancellation of interaction terms takes place. The interlayer Cu···Cu distance is only 7.88 Å, virtually the same as the intralayer Cu···Cu distance of 7.86 Å. More important than the Cu-Cu distances are the Br···Br contact distances between adjacent $CuBr_4^{2+}$ tetrahedra, since the exchange interaction occurs through the overlap of the bromide wave functions. Within the layer, the Br···Br separation is 4.35 Å, with only one Br···Br contact between any pair of copper sites in the layer, Fig. 2. Between the layers, the Br-Br separation is 4.83 Å, and there are two such contacts between each pair of interacting copper ions, Fig. 3. The resulting J'/J ratio of 0.08 is therefore a consequence of two identical interlayer interactions, each equal to $0.04J$.

E. Comparisons to other 2D QHAF's

To date, the compounds studied which approximate the 2D QHAF are few. A brief summary of these systems is given in Table V. Along with La_2CuO_4,[34] other compounds which have been studied include $Sr_2CuO_2Cl_2$,[28] copper formate (CuF4H),[32,35] copper formate urea (CuFUH),[36] and copper fluoride dihydrate.[37] Major studies of La_2CuO_4 include the neutron-scattering experiments of Hayden *et al.*[38] Much attention has been given to the complicated Néel transition near 300 K.[39] This magnetic transition is complicated by the structural transition near 500 K from tetragonal to orthorhombic symmetry which causes a canting of the local CuO_6 octahedra, therefore creating both a small intraplanar XY and a Dzyaloshinsky-Moria anisotropy. Knowledge of these anisotropies is essential to understanding the theory[40] and experiment[41] of the relaxation processes.

There is an absence of canting in $Sr_2CuO_2Cl_2$ which makes it a better realization of a 2D QHAF. A determination of the temperature dependence of the correlation length[28] found essentially perfect agreement between the data and the renormalized classical theory of Chakravarty *et al.*[29] However, no evidence was seen for the predicted crossover from the renormalized classical regime to quantum critical behavior at higher temperatures.

The nonoxide versions of the 2D QHAF's are characterized by much smaller exchange. This is an important advantage since certain experiments (EPR linewidth, magnetic specific heat, magnetization) are difficult to conduct on the oxides. However, each of these model compounds has its own set of limitations. The formate-based compounds, CuF4H and CuFUH, have two copper sites significantly canted one to another. Although, to our best knowledge, the only study of the EPR linewidth divergence has been done on CuF4H,[42] its conclusions are rendered suspect by the anisotropy contributions to the relaxation process. Copper fluoride dihydrate has no canting, but does have significant 3D interactions, as judged by its relatively high T_N/J ratio.[43]

The scarcity of well-characterized realizations of 2D QHAF's demonstrates a clear need for additional magnets with which to probe the behavior of this important class of quantum magnets. Desirable characteristics of the materials will include moderate exchange strengths, high local symmetries, and well-isolated magnetic layers. Our initial results presented here indicate that $(5CAP)_2CuBr_4$ and $(5MAP)_2CuBr_4$ are good candidates for studying the properties of 2D QHAF's. These systems have magnetic interactions that are in a desirable range for a variety of experiments. Although there is a transition to long-range order at relatively high temperature, temperatures above and below T_N may still show predominant 2D QHAF behavior as demonstrated by the agreement of our magnetization data with calculations of finite systems [see Fig. 6(b)].

From the perspective of molecular-based magnetism, what can be done to improve the 5CAP/5MAP family of 2D QHAF's? It would be good to lower the J'/J ratio so the interpretation of experimental data will be less affected by 3D crossover effects. Since the value of J' is determined by the interlayer Br···Br contacts, increasing the interlayer separation should have a dramatic impact upon J', without

significant influence on J. The interlayer spacing $\frac{1}{2}c$ is primarily determined by the length of the organic cations, from the 2-amino group to the substituent in the five position, Fig. 3. Replacing the chlorine ion in 5CAP with a larger ion (bromide, iodine, cyanide) may serve to push the layers further apart. Structural studies[12] with the 5-bromo substituent have shown the interlayer Br-Br contact distance has expanded to 4.99(6) Å from 4.83 Å in $(5CAP)_2CuBr_4$, while the contact distance within the layers has only increased to 4.396 Å from 4.35 Å [found in the $(5CAP)_2CuBr_4$]. Increasing the size of the five substituent led to changes in the key Br-Br contact distances which caused the expected changes in the magnetism for the $(5BAP)_2CuBr_4$ compound (5BAP=2-amino-5-bromopyridinium).[44] Changes in the Br-Br contacts resulted in $J=6.9(1)$ K, $T_N=3.8(2)$ K causing a moderate reduction in the T_N/J ratio to 0.57.

Increasing the size of the five substituent of the pyridine ring still further, by use of iodine, forces the complex to a completely new structure. The compound $(5IAP)_2CuBr_4\cdot 2H_2O$ (5IAP=2-amino-5-iodiopyridinium) consists of ladders of close-packed $CuBr_4^{2-}$ groups with magnetic interactions $J_{rung}=13$ K and $J_{rail}=1$ K.[45]

Another family of 2D QHAF's, with better 3D isolation than the $CuBr_4$ compounds, is also under investigation by our group. These compounds consist of Cu^{2+} ions mutually linked by neutral pyrazine molecules (pz, $C_4H_4N_2$) into antiferromagnetic layers:[12,46] $Cu(pz)_2(ClO_4)_2$, $Cu(pz)_2(BF_4)_2$, and $[Cu(pz)_2(NO_3)](PF_6)$. The exchange strengths, 10.5–17 K, are stronger and the 3D isolation is better, $T_N/J\approx 0.25$, than the $CuBr_4$ compounds. The improvement in the critical ratio is due to the wide separation of the layers by the interleaved anions. Full reports of synthesis, structures, and magnetic properties of these compounds are in preparation.

ACKNOWLEDGMENTS

The authors would like to acknowledge Ward Robinson, University of Canterbury, for assistance with the x-ray data collection, Dan Reich, Johns Hopkins University, and Joseph Budnick, University of Connecticut-Storrs, for the use of their SQUID magnetometers, and M. Sorai, Microcalorimetry Center - Osaka University, for his work on the specific heat. We had useful discussions with E. Manousakis and Martin Graven as well as with M. Troyer who let us use his unpublished results on the magnetization curve of the 2D QHAF. We gratefully acknowledge many valuable conversations with R. Willett. A portion of this work was performed at the National High Magnetic Field Laboratory, which is supported by SF Cooperative Agreement No. DMR-9527035 and by the State of Florida. We received support from the NSF through Grant Nos. DMR-9006470 and DMR-9803813.

[1] R. J. Birgeneau, Am. J. Phys. **58**, 28 (1990).
[2] A. Sokol and D. Pines, Phys. Rev. Lett. **71**, 2813 (1993).
[3] E. Manousakis, Rev. Mod. Phys. **63**, 1 (1991).
[4] M. S. Yang and K. Mütter, Z. Phys. B: Condens. Matter **104**, 117 (1997).
[5] M. E. Zhitomirsky and T. Nikuni, Phys. Rev. B **57**, 5013 (1998).
[6] M. E. Zhitomirsky and A. L. Chernyshev, Phys. Rev. Lett. **82**, 4536 (1999).
[7] O. Kahn, *Molecular Magnetism* (VCH, New York, 1993).
[8] H. Place and R. Willett, Acta Crystallogr., Sect. C: Cryst. Struct. Commun. **C43**, 1050 (1987).
[9] P. Zhou, J. Drumheller, G. Rubenacker, K. Halvorson, and R. Willett, J. Appl. Phys. **69**, 5804 (1991).
[10] R. Willett, H. Place, and M. Middleton, J. Am. Chem. Soc. **110**, 8639 (1988).
[11] T. Matsumoto, Y. Miyazaki, A. A. Albrecht, C. P. Landee, M. M. Turnbull, and M. Sorai, J. Phys. Chem. B **104**, 9993 (2001).
[12] M. M. Turnbull, A. S. Albrecht, G. B. Jameson, and C. P. Landee, Mol. Cryst. Liq. Cryst. Sci. Technol., Sect. A **335**, 245 (1999).
[13] R. B. Griffiths, Phys. Rev. **133**, A768 (1964).
[14] M. Troyer (private communication).
[15] C. Poole and H. Farach, *The Theory of Magnetic Resonance* (Wiley, New York, 1972).
[16] P. Hammar, D. Dender, D. Reich, A. Albrecht, and C. Landee, J. Appl. Phys. **81**, 4615 (1997).
[17] G. S. Rushbrooke, G. A. Baker, and P. J. Wood, *Phase Transitions and Critical Phenomena* (Academic, New York, 1974).
[18] M. Takahashi, Phys. Rev. B **40**, 2494 (1989).
[19] R. R. P. Singh and M. P. Gelfand, Phys. Rev. B **42**, 996 (1990).
[20] J.-K. Kim and M. Troyer, Phys. Rev. Lett. **80**, 2705 (1998).
[21] M. S. Makivić and H.-Q. Ding, Phys. Rev. B **43**, 3562 (1991).
[22] S. Eggert, I. Affleck, and M. Takahashi, Phys. Rev. Lett. **73**, 332 (1994).
[23] R. Willett, Inorg. Chem. **25**, 1918 (1986).
[24] J. Bonner and M. Fisher, Phys. Rev. **135**, A640 (1964).
[25] *Low Dimensional Systems of Semiconductors and Magnetic Materials in Very High Magnetic Fields up to 500 T* (World Scientific, Singapore, 1995).
[26] L. J. Dejongh, W. D. V. Amstel, and A. R. Miedema, Physica (Amsterdam) **58**, 277 (1972).
[27] R. Navarro, in *Magnetic Properties of Layered Transition Metal Compounds*, edited by L. D. Jongh (Kluwer Academic Press, Dordecht, 1990), p. 105.
[28] M. Greven, R. Birgeneau, Y. Endoh, M. Kastner, M. Matsuda, and G. Shirane, Z. Phys. B: Condens. Matter **96**, 465 (1995).
[29] S. Chakravarty, B. I. Halperin, and D. R. Nelson, Phys. Rev. Lett. **60**, 1057 (1988).
[30] P. Hasenfratz and F. Niedermayer, Z. Phys. B: Condens. Matter **92**, 91 (1993).
[31] B. B. Beard, R. J. Birgeneau, M. Greven, and U.-J. Wiese, Phys. Rev. Lett. **80**, 1742 (1998).
[32] H. M. Ronnow, D. F. McMorrow, and A. Harrison, Phys. Rev. Lett. **82**, 3152 (1999).
[33] J. Villain and J. M. Loveluck, J. Phys. (France) Lett. **88**, L77 (1977).
[34] Y. Endoh, G. Shirane, R. J. Birgeneau, P. M. Richards, and S. L. Holt, Phys. Rev. Lett. **32**, 170 (1974).

[35] S. Clarke and A. Harrison, J. Phys.: Condens. Matter **4**, 6217 (1992).
[36] K. Yamagata and H. Abe, J. Magn. Magn. Mater. **31-34**, 1179 (1983).
[37] K. Koyama, H. Nobumasa, and M. Matsura, J. Phys. Soc. Jpn. **56**, 1553 (1987).
[38] S. M. Hayden, G. Aeppli, R. Osborn, A. D. Taylor, T. G. Perring, S. W. Cheong, and Z. Fisk, Phys. Rev. Lett. **67**, 3622 (1991).
[39] D. E. MacLaughlin, J. P. Vithayathil, H. B. Brom, J. C. J. M. de Rooy, P. C. Hammel, P. C. Canfield, A. P. Reyes, Z. Fisk, J. D. Thompson, and S-W. Cheong, Phys. Rev. Lett. **72**, 760 (1994).
[40] S. Chakravarty, M. P. Gelfand, P. Kopietz, R. Orbach, and M. Wollensak, Phys. Rev. B **43**, 2796 (1991).
[41] T. Imai, C. P. Slichter, K. Yoshimura, M. Katoh, and K. Kosuge, Phys. Rev. Lett. **71**, 1254 (1993).
[42] T. G. Castner and M. S. Seehra, Phys. Rev. B **47**, 578 (1993).
[43] S. C. Abrahams, J. Chem. Phys. **36**, 56 (1962).
[44] F. M. Woodward, C. P. Landee, J. Giantsidis, M. M. Turnbull, and C. Richardson, Inorg. Chim. Acta **324**, 324 (2001).
[45] C. Landee, M. Turnbull, C. Galeriu, J. Giantsidis, and F. Woodward, Phys. Rev. B **63**, 100402 (2001).
[46] A. S. Albrecht, C. P. Landee, Z. Slanic, and M. M. Turnbull, Mol. Cryst. Liq. Cryst. Sci. Technol., Sect. A **305**, 333 (1997).
[47] Y. Endoh, K. Yamada, R. J. Birgeneau, D. R. Gabbe, H. P. Jenssen, M. A. Kastner, C. J. Peters, P. J. Picone, T. R. Thurston, J. M. Tranquada, G. Shirane, Y. Hidaka, M. Oda, Y. Enomoto, M. Suzuki, and T. Murakami, Phys. Rev. B **37**, 7443 (1988).
[48] R. Coldea, S. M. Hayden, G. Aeppli, T. G. Perring, C. D. Frost, T. E. Mason, S.-W. Cheong, and Z. Fisk, Phys. Rev. Lett. **86**, 5377 (2001).
[49] H. M. Ronnow, D. F. McMorrow, R. Coldea, A. Harrison, I. D. Youngson, T. G. Perring, G. Aeppli, O. Syljuasen, K. Lefmann, and C. Rischel, Phys. Rev. Lett. **87**, 037202 (2001).
[50] H. Algra, L. de Jongh, and R. Carlin, Physica B & C **93B**, 24 (1978).
[51] M. D. Lumsden, B. C. Sales, D. Mandrus, S. E. Nagler, and J. R. Thompson, Phys. Rev. Lett. **86**, 159 (2001).